Supporting Information

Sheng et al. 10.1073/pnas.1800719115

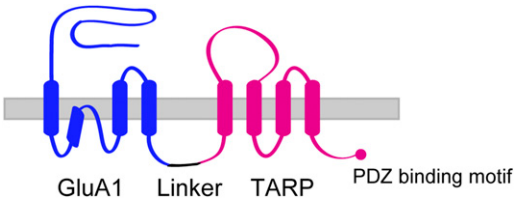

Fig. S1. The diagram of construction of the GluA1-TARP tethered receptor. The C-tail of GluA1 (blue) was fused to the N terminus of TARP (red) with a short segment of linker sequence (black). The PDZ-binding motif is highlighted by a filled circle.

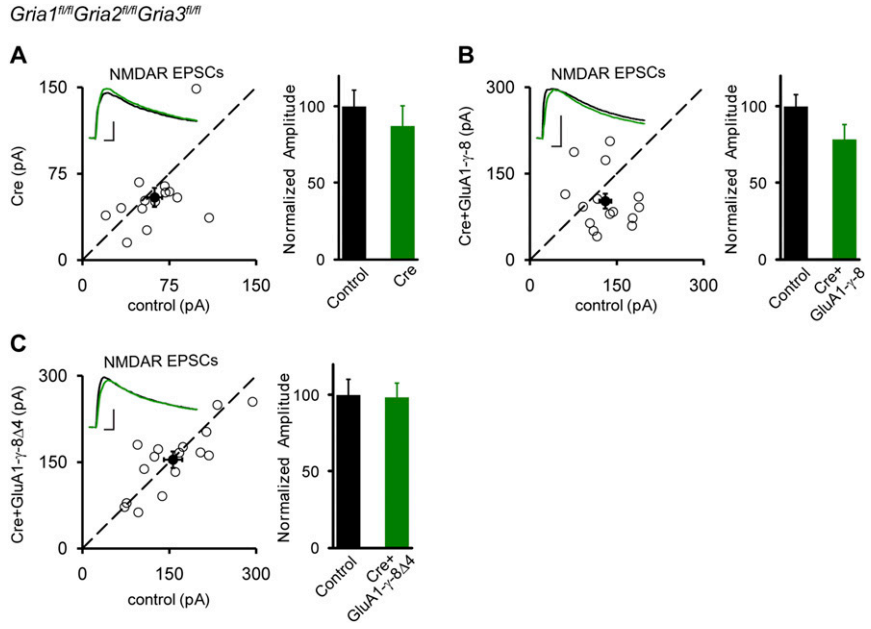

Fig. S2. NMDAR-mediated synaptic transmission is intact in experiments where AMPARs are knocked out or replaced with GluA1-TARP tethered receptors. Simultaneous dual whole-cell recordings from a transfected CA1 pyramidal neuron and a neighboring wild-type one from P17–P21 acute slices as in Fig. 1 *A*–*C*. Open and filled circles represent amplitudes of NMDAR-EPSCs (the current amplitudes were measured 100 ms after stimulation) for single pairs and mean ± SEM, respectively. (*Insets*) Sample current traces from control (black) and experimental (green) cells. (Scale bars: 100 pA and 25 ms for representative traces.) Bar graphs show normalized EPSC amplitudes (mean ± SEM) (Cre: *A*, $n = 14$, 87.31 ± 13.21% control, $P > 0.05$; Cre+GluA1-γ-8: *B*, $n = 15$, 78.46 ± 9.91% control, $P > 0.05$; Cre+GluA1-γ-8Δ4: *C*, $n = 16$, 98.49 ± 9.13% control, $P > 0.05$) presented in scatter plots. All of the statistical analyses are compared with respective control neurons by the two-tailed Wilcoxon signed-rank sum test.

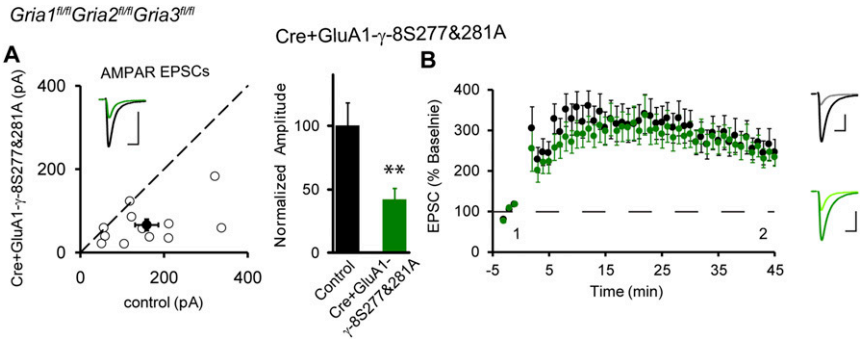

Fig. S3. Phosphorylation of γ-8 is involved in synaptic trafficking of the tethered GluA1 receptor but not required for LTP. The endogenous AMPARs were replaced with GluA1-γ-8(S277&281A) as in Fig. 1*B*. (*A*) Open and filled circles represent amplitudes of AMPAR-EPSCs for single pairs and mean ± SEM, respectively. (*Insets*) Sample current traces from control (black) and experimental (green) cells. (Scale bars: 100 pA and 25 ms for representative traces.) Bar graphs show normalized EPSC amplitudes (mean ± SEM) (n = 12, 41.84 ± 8.50% control, $^{**}P < 0.005$) presented in scatter plots. (*B*) LTP of GluA1-γ-8(S277&281A) replacement neurons (n = 10) is similar to neighboring wild-type cells. The data are shown as the percentage of the respective baseline before LTP induction (mean ± SEM). Sample traces show EPSCs before and 30 min after LTP induction in paired control (black) and replacement neurons (green). (Scale bars: 100 pA and 25 ms.) All of the statistical analyses are compared with respective control neurons by the two-tailed Wilcoxon signed-rank sum test.

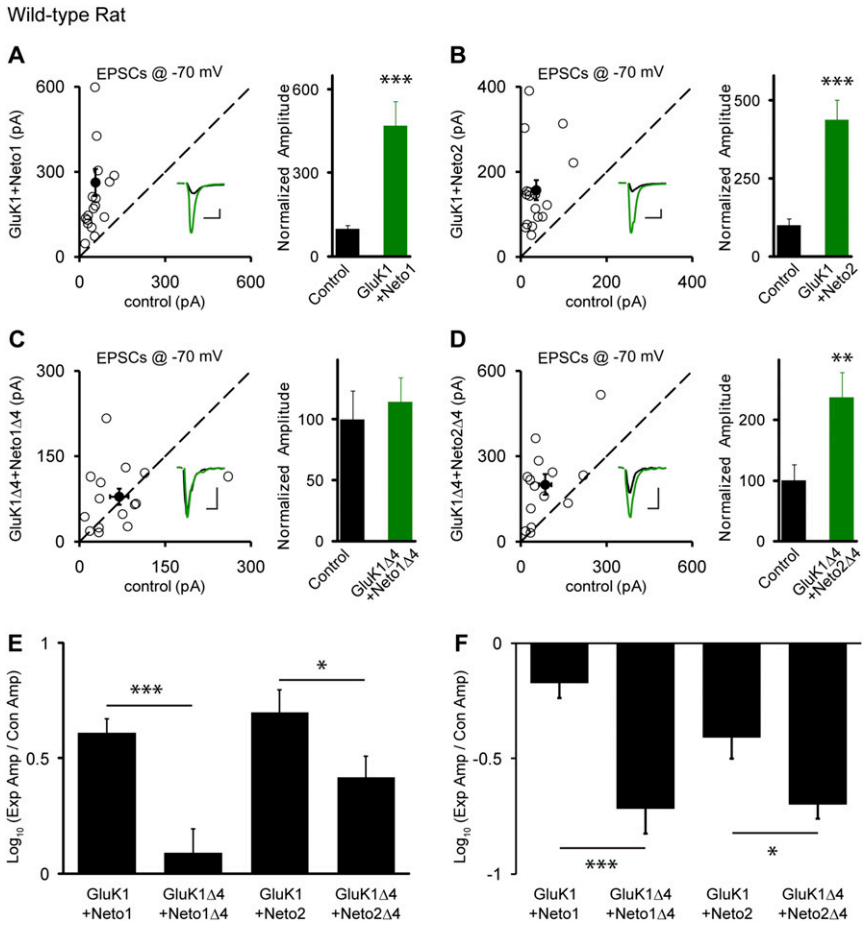

Fig. S4. PDZ-binding motif-mediated interaction is required for synaptic targeting of GluK1/Neto receptors. Rat hippocampal slice cultures were biolistically transfected with indicated constructs, and dual whole-cell recordings were applied to examine evoked EPSCs. (*A–D*) Open and filled circles represent amplitudes of EPSCs for single pairs and mean ± SEM, respectively. (*Insets*) Sample current traces from control (black) and experimental (green) cells. [Scale bars: 100 pA and 25 ms (*A* and *B*) and 50 pA and 25 ms (*C* and *D*) for representative traces.] Bar graphs show normalized EPSC amplitudes (mean ± SEM) (GluK1/Neto1: *A*, $n = 19$, 470.65 ± 85.60% control, $^{***}P < 0.0005$; GluK1/Neto2: *B*, $n = 17$, 689.52 ± 195.16% control, $^{***}P < 0.0005$; GluK1Δ4/Neto1Δ4: *C*, $n = 15$, 114.09 ± 20.36% control, $P > 0.05$; GluK1Δ4/Neto2Δ4: *D*, $n = 14$, 236.51 ± 41.54% control, $^{**}P < 0.005$) presented in scatter plots. All of the statistical analyses are compared with respective control neurons by the two-tailed Wilcoxon signed-rank sum test. (*E*) Logarithm summary of the EPSC amplitudes ratio between the experimental and respective control neurons (mean ± SEM) for the above four experimental groups [GluK1/Neto1 (0.61 ± 0.06) vs. GluK1Δ4/Neto1Δ4 (0.09 ± 0.11), $^{***}P < 0.001$; GluK1/Neto2 (0.70 ± 0.10) vs. GluK1Δ4/Neto2Δ4 (0.42 ± 0.09), $^{*}P < 0.05$]. All statistical analyses of the different groups are tested using the Mann–Whitney *U* test. It should be noted that the raw data of GluK1/Neto1 and GluK1/Neto2 are reused from our previous study (26). (*F*) Logarithm summary of the EPSC amplitudes ratio between the experimental and respective control neurons (mean ± SEM) for the four replacement experimental groups in Fig. 3 [GluK1/Neto1 (–0.17 ± 0.06) vs. GluK1Δ4/Neto1Δ4 (–0.72 ± 0.11), $^{***}P < 0.001$; GluK1/Neto2 (–0.41 ± 0.09) vs. GluK1Δ4/Neto2Δ4 (–0.70 ± 0.06), $^{*}P < 0.05$]. All statistical analyses of the different groups are tested using the Mann–Whitney *U* test.

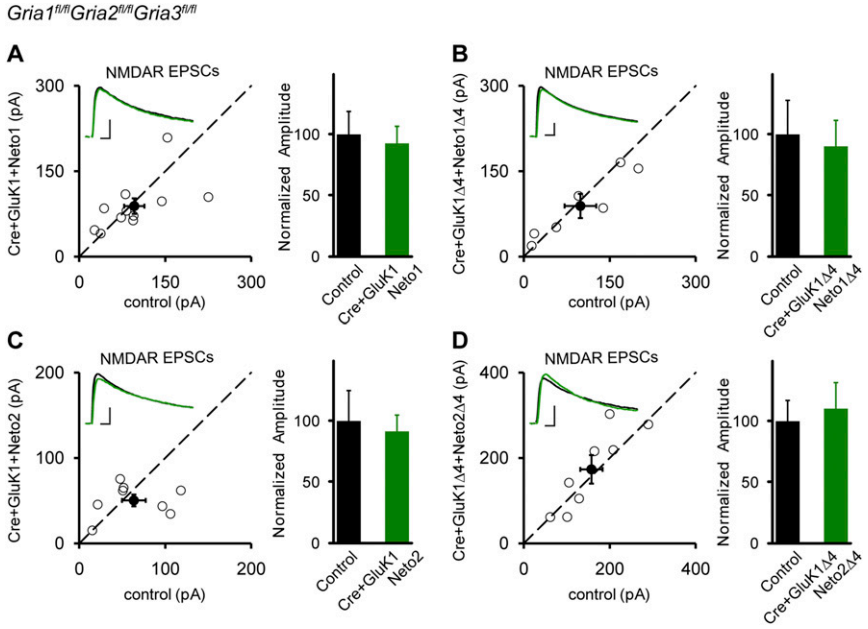

Fig. S5. NMDAR-mediated synaptic transmission is intact in experiments where AMPARs were replaced with KARs. The same experimental procedure was followed as in Fig. 3 *A1–D1* except that open and filled circles represent amplitudes of NMDAR-EPSCs (the current amplitudes were measured 100 ms after stimulation) for single pairs and mean ± SEM, respectively. *Insets* show sample current traces from control (black) and experimental (green) cells. (Scale bars are 50 pA and 25 ms for representative traces.) Bar graphs show normalized EPSC amplitudes (mean ± SEM) (GluK1/Neto1: *A*, $n = 11$, 92.39 ± 14.28% control, $P > 0.05$; GluK1Δ4/Neto1Δ4: *B*, $n = 7$, 89.96 ± 21.60% control, $P > 0.05$; GluK1/Neto2: *C*, $n = 8$, 91.55 ± 13.09% control, $P > 0.005$; GluK1Δ4/Neto1Δ4: *D*, $n = 8$, 110.02 ± 21.19% control, $P > 0.05$) presented in scatter plots. All of the statistical analyses are compared with respective control neurons by the two-tailed Wilcoxon signed-rank sum test.